Available online at www.sciencedirect.com
SCIENCE DIRECT®
Journal of volcanology and geothermal research
ELSEVIER
Journal of Volcanology and Geothermal Research 129 (2004) 199–217
www.elsevier.com/locate/jvolgeores

The role of extensional structures on experimental calderas and resurgence

V. Acocella [a,*], R. Funiciello [a], E. Marotta [b], G. Orsi [b], S. de Vita [b]

[a] *Dip. Scienze Geologiche Universita Roma TRE, Largo S.L. Murialdo, 1-00146 Roma, Italy*
[b] *Osservatorio Vesuviano, Via Diocleziano, 328, 80124, Napoli, Italy*

Received 1 July 2002; accepted 14 February 2003

Abstract

The structure and shape of collapses and resurgences is often controlled by pre-existing discontinuities, such as normal faults in rift zones. In order to study the role of extensional structures on collapse and resurgence, we used analogue models. Dry sand simulated the brittle crust; silicone, located at the base of the sand-pack, simulated magma. In the experiments, regional extension pre-dated collapse or resurgence, forming normal faults in a graben-like structure; the graben was filled with additional sand, simulating post-rift deposits. A piston then moved the silicone downward or upward, inducing collapse or resurgence within the previously deformed sand. The collapses showed an ellipticity (length of minor axis/length of major axis) between 0.8 and 0.9, with the major axis parallel to the extension direction. The partial reactivation of the pre-existing normal faults was observed during the development of the caldera reverse faults, which, conversely to what was expected (from experiments without pre-existing extension), became partly inward dipping. Resurgence showed an elongation of the uplifted part, with the main axis perpendicular to the extension direction. At depth, pre-existing normal faults were partly reactivated by the reverse faults formed during resurgence; these locally became outward dipping normal faults. A total reactivation of pre-existing faults was also observed during resurgence. The experiments suggest that the observed elongation of calderas and resurgences is the result of the reactivation of pre-existing structures during differential uplift. Such a reactivation is mainly related to the loss in the coefficient of friction of the sand. The results suggest that elliptic calderas and resurgences in nature may develop even from circular magma chambers.

Keywords: extensional structures; caldera; resurgence; analogue models; reactivation

1. Introduction

Collapse calderas and resurgent domes are common features in volcanic systems and have been classically interpreted in the light of an evolution characterised by regional tumescence, major eruption and caldera collapse and intracaldera resurgent doming (Smith and Bailey, 1968; Henry and Price, 1984; Newhall and Dzurisin, 1988). Calderas and domes are commonly related to inflation–deflation processes inside magma chambers (Smith and Bailey, 1968; Lipman,

* Corresponding author. Fax: +39-06-54888201.
E-mail addresses: acocella@uniroma3.it (V. Acocella), funiciel@uniroma3.it (R. Funiciello), marotta@ov.ingv.it (E. Marotta), orsi@osve.ingo.it (G. Orsi), devita@osve.ingo.it (S. de Vita).

0377-0273/03/$ – see front matter © 2003 Elsevier B.V. All rights reserved.
doi:10.1016/S0377-0273(03)00240-3

1984; Newhall and Dzurisin, 1988; Lipman, 1997).

Calderas have been related to the removal of magma from the chamber (Williams, 1941; Smith, 1979; Druitt and Sparks, 1984; Scandone, 1990; Lipman, 1997), to the excess of magma pressure in sill-like chambers (Komuro, 1987; Gudmundsson, 1988; Gudmundsson et al., 1997; Gudmundsson, 1998), or to the weight of underlying intrusions (Walker, 1988). Resurgence consists of the uplift of part of a volcanic system, due to the ascent of silicic magma (Smith and Bailey, 1968; Lipman, 1984; Marsh, 1984). Resurgence may form resurgent blocks (Civetta et al., 1988; Orsi et al., 1991; Acocella and Funiciello, 1999) or domes (Bailey et al., 1976; Lipman, 1984; Self et al., 1986) depending upon the aspect ratio (width/thickness) of the crust overlying the magma chamber; resurgent blocks form for aspect ratios $\sim$1, whereas domes form for aspect ratios $\sim$0.4 (Acocella et al., 2001a).

The structure of calderas and resurgences has been recently investigated through analogue models (Marti et al., 1994; Kennedy et al., 1999; Acocella et al., 2000; Roche et al., 2000; Acocella et al., 2001a; Acocella et al., 2001b; Walter and Troll, 2001; Troll et al., 2002). These experiments show similar structures: high angle reverse faults border calderas and resurgences, whereas normal faults form subsequently. The reverse faults are the structural boundaries of calderas and resurgences, mechanically consistent with a differential uplift; conversely, the normal faults are a result of the gravitational collapse induced by the reverse faults (e.g. Acocella et al., 2000, and references therein).

Despite the observed similar deformation pattern, these models were the result of a near-field stress, induced by the intrusion, and did not take into account the role of far-field (i.e. regional) stresses. These may, in fact, induce significant deviations from the observed patterns in different ways: through pre-existing regional structures (inherited strain), which may influence the propagation of the stresses or also be reactivated during collapse and resurgence; through the direct control of the regional stresses (simultaneous stress) during collapse and resurgence. As most of the resurgences and calderas are located in extensional settings, extensional tectonics is the most representative far-field stress to consider for any simulation. Examples of calderas and resurgences in different (intraplate rift, oceanic ridge, continental rift) extensional settings are reported in Fig. 1.

In order to evaluate the role of pre-existing extensional structures on differential uplifts in volcanic areas, we performed analogue models. Here we present the results of the experiments, where we consider the role of pre-existing regional extensional structures on collapse and resurgence. The effect of a simultaneous extensional stress on resurgence was previously investigated (Withjack and Scheiner, 1982), showing fractures resulting from the superimposition of a regional and local stress field. Here we consider the effect of an inherited extensional strain on collapse and resurgence, where extension is simulated only before, not during, collapse or resurgence. This fact is supported by the evidence that collapses and resurgences (strain rates usually between 10^{-5}–10^{-12} s^{-1}) are much faster than regional tectonics (strain rates usually $\sim 10^{-15}$ s^{-1}). We first describe the effect on collapse, then on resurgence and finally on the superimposition of resurgence over collapse. Our results simulate only large (vertical displacement from several tens of metres to thousands of metres) collapses or resurgences. However, a detailed comparison with nature is beyond the scope of this paper and is only briefly addressed. The results highlight the reactivation of pre-existing regional normal faults on the deformation pattern and its role on the ellipticity of calderas and resurgences.

2. Experimental procedure

2.1. Scaling

Models have to be geometrically, kinematically and dynamically scaled, following the principles discussed by Hubbert (1937) and Ramberg (1981). We chose a length ratio between model and nature $z^* = 10^{-5}$ (1 cm in the model corresponds to 1 km in nature; Table 1). The densities of natural rocks (2000–2700 kg m^{-3}) and of the

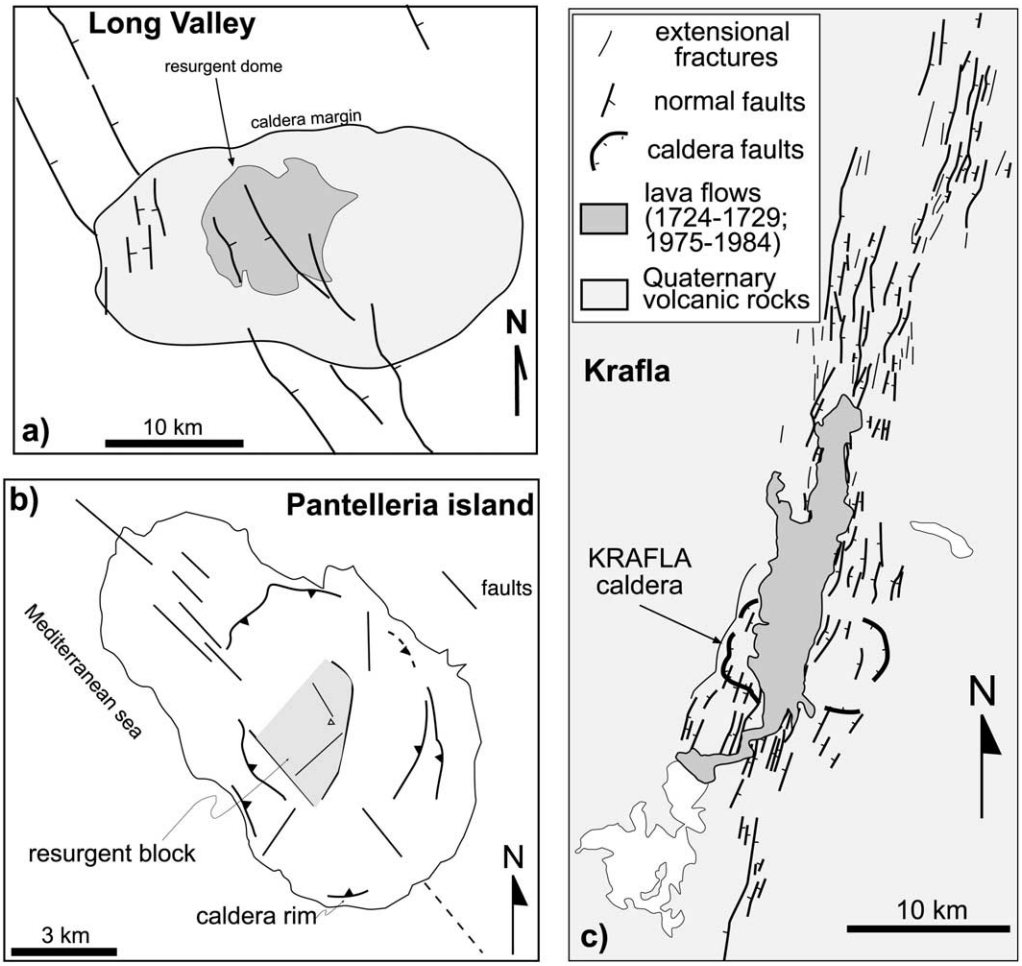

Fig. 1. Examples of calderas and resurgences in extensional settings. (a) Sketch of the Long Valley caldera and resurgent dome, California, on the western side of the Basin and Range extensional Province (modified after Goldstein and Stein, 1988). (b) Structural map of Pantelleria island, located along the Rift in the Straits of Sicily (Italy), showing a resurgent caldera (modified after Civetta et al., 1988). (c) Structural map of the Krafla caldera, within the oceanic rift of Iceland (modified after Opheim and Gudmundsson, 1989).

experimental materials commercially available (900–1800 kg m^{-3}) impose a density ratio $\rho^* \sim 0.5$. Since the models were run at 1 g, the gravity ratio $g^* = 1$. These ratios imply that the stress ratio between model and nature is $\rho^* g^* z^* \sim 5 \times 10^{-6}$.

We assumed a Mohr–Coulomb failure criterion for the rocks in the brittle crust, with an angle of internal friction $\phi = 30°$ and a mean cohesion $c = 10^7$ Pa. Cohesion, having the dimensions of a stress, must be scaled at approximately 5×10^{-6} in the experiments; this requires the use of material with $c = 50$ Pa to simulate the brittle crust. For this purpose, we used well sorted, round grain, dry quartzose sand, with $\phi = 37°$ and cohesion of few hundreds of Pa; its rheological properties and use as analogue material are discussed in Krantz (1991) and Schellart (2000).

The simulation of magma has to take the viscosities, the related strain rates and timescales into account. Newtonian silicone putty, with viscosity $\sim 10^4$ Pa s, simulated the ductile behaviour of magma (Weijermars et al., 1993; Merle and Vendeville, 1995; Donnadieu and Merle, 1998;

Table 1
Scaling procedure adopted in the experiments

Brittle behaviour

Length ratio	Gravity ratio	Density ratio	Stress ratio
$L^* = L_{mod}/L_{nat} = 10^{-5}$	$g^* = 1$	$\rho^* = 0.5$	$\sigma^* = \rho^* g^* L^* = 5 \times 10^{-6}$

Ductile behaviour

Natural viscosity (μ) (Pa s)	Viscosity ratio (μ*) $\mu_{mod} = 10^4$ Pa s	Strain rate ratio $e^* = \sigma^*/\mu^*$	Time ratio $t^* = 1/e^*$	Velocity ratio $v^* = e^* L^*$	Natural velocity $V_{nat} = m/h$
10^4	1	5×10^{-6}	2×10^5	5×10^{-11}	1×10^8
10^7	10^{-3}	5×10^{-3}	2×10^2	5×10^{-8}	1×10^5
10^{11}	10^{-7}	5×10^1	2×10^{-2}	5×10^{-4}	1×10^1
10^{15}	10^{-11}	5×10^5	2×10^{-6}	5	1×10^{-3}
10^{18}	10^{-14}	5×10^8	2×10^{-9}	5×10^3	1×10^{-6}

The scaling for the brittle crust imposes the use of cohesionless sand as analogue material. Newtonian silicone putty has been used to simulate magma. The table provides the simulated viscosity, strain rate, timescale and velocity ratios between models and nature.

Hailermariam and Mulugeta, 1998; Merle, 1998). Magma viscosities vary widely, even within a very limited range of temperatures (Talbot, 1999). The corresponding wide range of viscosity ratios between model and nature are listed in Table 1; for a given viscosity and the imposed stress ratio, the related strain rate, timescale and velocity ratios are shown.

The extent to which the experimental results are applicable is limited by current knowledge of such natural parameters as viscosities, timescales and strain rates. Given the possible range of these values in nature, a single experiment might be associated with different equivalents in nature, characterised by different viscosities, timescales and strain rates (Table 1). The aim of the experiments is thus not to simulate specific cases; the goal is rather to understand the overall mechanism of deformation, which might be valid for a wide range of natural cases.

2.2. Experimental apparatus

The experimental apparatus consists of three parts: a cylinder with a piston inside, connected to an engine; a table, with a hole in correspondence with the circular (diameter $D = 5$ cm) nozzle of the underlying cylinder; a sliding plate above the table, attached to a vertical wall connected to a second engine (Fig. 2). Silicone, intended to simulate a magmatic body at depth, fills the cylinder up to the level of the table. Horizontal layers of sand, intended to simulate the brittle crust overlying a magma chamber, are placed partly on the sliding plate, partly on the table.

Extension is first induced in the sand-pack. Pulling the plate with the engine outwards induces in fact a velocity discontinuity (VD) at the edge of the sliding plate; this is responsible for the development of extensional structures within the sand-pack. The VD induced extension throughout the sand above the silicone. Additional horizontal layers of sand are placed at intervals (corresponding to 1 cm of extension) within the depression formed by the migrating VD in order to simulate syn-rift deposits and provide a horizontal topography before collapse or resurgence, in order to study the deformation process without topographic controls.

After extending the sand-pack, the extension engine is switched off and collapse or resurgence is simulated with the downward or upward movement of the piston within the cylinder. This induces the respective fall and rise of silicone and further deforms the overlying sand-pack. The purpose of the experiments is to study the deformation pattern induced by the vertical movement of the silicone within a pre-fractured sand-pack under a previous regional extension.

We tested the role of the following five parameters (Fig. 2): (1) the thickness (T) of the sand-pack (between 3 and 7 cm), (2) the total amount

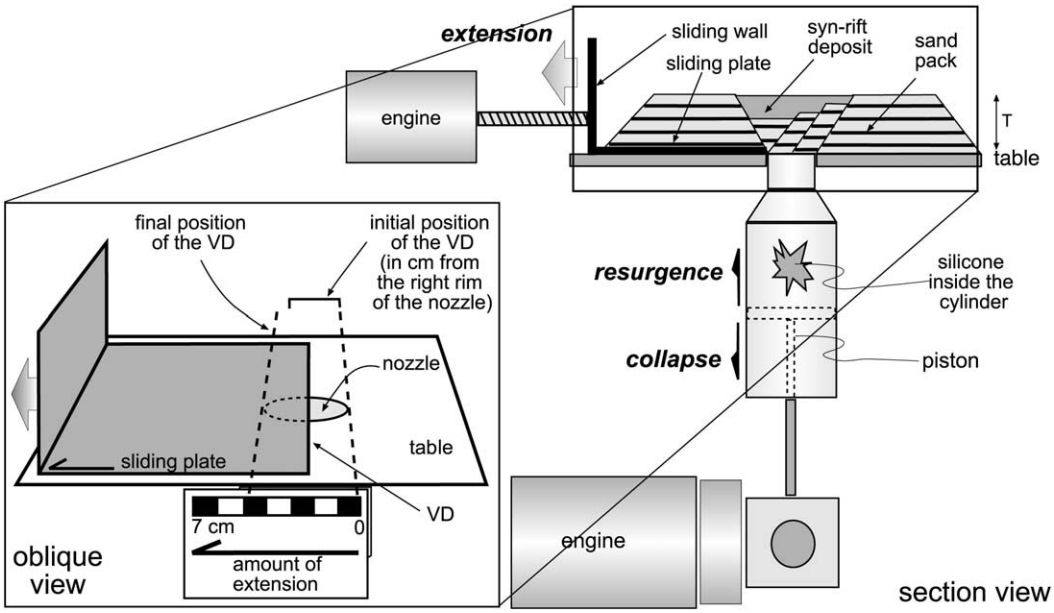

Fig. 2. Section view of the experimental apparatus. Silicone putty is placed inside the cylinder. Extension, controlled by the outward sliding of a mobile table above a plate, induces normal faults within the sand-pack. The extensional zone (graben) is filled with sand. The downward or upward movement of the piston generates collapse or resurgence in the sand-pack. Inset shows an oblique view of the sliding VD, responsible for the nucleation of normal faults: extension is measured in cm from the initial position of the VD with regard to the right rim of the nozzle.

Table 2
Main imposed parameters and observed features for calderas and resurgences

Experiment	Imposed parameters					Observed features	
Collapse	T	Extension		Duration (min)		Eccentricity	Reactivated structures
	(cm)	(cm)		t_{est}	t_{col}		
CALTEC 3	5	7	0	84	168	0.88 ± 0.04	1
CALTEC 4	7	7	0	90	161	0.85 ± 0.06	1
CALTEC 5	5	5.3	0	60	157	0.80 ± 0.04	2
CALTEC 6	5	5.3	0	63	63	0.81 ± 0.02	2
CALTEC 7	5	5.2	1.5	63	65	0.90 ± 0.05	1
CALTEC 8	5	5.2	1.5	62	186	0.90 ± 0.07	1
CALTEC 11	5	5	0	64	180	0.81 ± 0.06	2
CALTEC 12	5	1.3	4	18	187	0.90 ± 0.06	1
Resurgence	T	Extension		Duration (min)		Eccentricity	Reactivated structures
	(cm)	(cm)		t_{est}	t_{res}		
CALTEC 9	5	5	0	54	191	0.89 ± 0.04	1 (vertical fault)
CALTEC 10	3	3	0	64	183	1 ± 0.06	0 (inward dipping fault)
CALTEC 13	5	1.3	4	15	240	0.83 ± 0.05	1 (outward dipping fault)

In the 'extension' column, the left line refers to the total amount of extension and the right line to the distance of the VD from the right edge of the nozzle at the onset of extension.

of regional extension (i.e. the amount of sliding of the mobile wall; between 1.3 and 7 cm), (3) the location of the VD with regard to the circular nozzle at the base of the sand-pack (in cm, starting from the right rim of the nozzle, as in Fig. 2), (4) the time of collapse (t_{col}), and (5) the time of resurgence (t_{res}). Extension velocity was $\sim$50 mm h^{-1}. The sand-pack alone was extended and extension did not affect the underlying silicone. Collapse and resurgence velocities were $\sim$5 mm h^{-1} and running times were between 60 and 250 min.

Three sets of experiments were performed (Table 2). In the first set, the downward movement of the piston simulated collapse in the upper crust after regional extension. In the second, upward movement simulated resurgence after regional extension. In the third, the superimposition of resurgence over collapse after regional extension was studied. At the end of the experiments, additional sand was placed onto the model surface and then leveled, in order to preserve topography. The model was then saturated with water and cut into cross sections.

3. Experimental results

3.1. Set 1: extension and collapse

The first set of (eight) experiments simulates collapse calderas within a sand-pack with extensional structures; here we describe two representative experiments (CALTEC 3 and CALTEC 5).

Experiment CALTEC 3 has $T = 5$ cm, total duration of extension (from the onset of the extension to the offset of extension) $t_{ext} = 84'$ (min), for an extension of 7 cm, the initial position of the VD at the right rim of the 5-cm-wide nozzle and the total duration of collapse (from the offset of extension to the offset of collapse) $t_{col} = 168'$ (Fig. 3). The first stage of deformation was characterised by extension. This, at $t_{ext} \sim 15'$, formed two-opposite verging normal faults nucleated along the VD; The normal fault nucleated from the VD above the sliding plate and dipping towards the table is called 'synthetic', whereas we term the normal fault nucleated from the VD above the table and dipping towards the sliding plane 'antithetic' (Fig. 3a). These faults bordered a linear depression, a graben-like structure, located above the VD. Increasing the extension induced the further development of the synthetic fault, attached to the VD, while a new antithetic fault formed, along the migrating VD, at constant intervals every $\sim$1 cm of extension; as a consequence of the migration of the VD, the previous antithetic normal fault became locked (Fig. 3b). Further extension increased the displacement on the synthetic fault and formed additional antithetic normal faults, following the migration of the VD (Fig. 3c); the dip of these faults is $57° \pm 5°$.

This experiment was characterised by 7 cm of extension; in this way, the area above the nozzle, which will subsequently be affected by collapse, was completely pre-fractured. A section of this final stage of extension in CALTEC 3 is shown in Fig. 3d. The resulting graben had the synthetic normal fault accommodating all the deformation on one side and 6 antithetic normal faults accommodating extension on the opposite side; these normal faults are here termed as 'regional faults'. The graben is then filled with sand.

Once the extending engine was stopped, the collapse engine started. As a result of the downward movement of the piston, silicone sank within the cylinder. The map view of CALTEC 3 at $t_{col} = 40'$ shows a $\sim$4-cm-wide depression (Fig. 3e), with an eccentricity $E = L_{min}/L_{max}$ (where L_{min} is the length of the minor axis of the ellipse and L_{max} is the length of the major axis) $= 0.88 \pm 0.04$; the major axis of the ellipse is parallel to the extension direction. The further sink of the silicone forms an outer concentric depression starting at $t_{col} \sim 120'$. The final stage of deformation ($t_{col} = 170'$), beyond which no significant variation of the deformation pattern is observed, shows a fully developed outermost depression (Fig. 3f); although its right side partly follows a straight path (arrow in Fig. 3f), this depression is subcircular.

The section of the experiment, parallel to the extension direction and in correspondence with the diameter of the caldera, is shown in Fig. 3g. The correct evaluation of the deformation pattern in Fig. 3g was made through the comparison with sections from analogue models of calderas with-

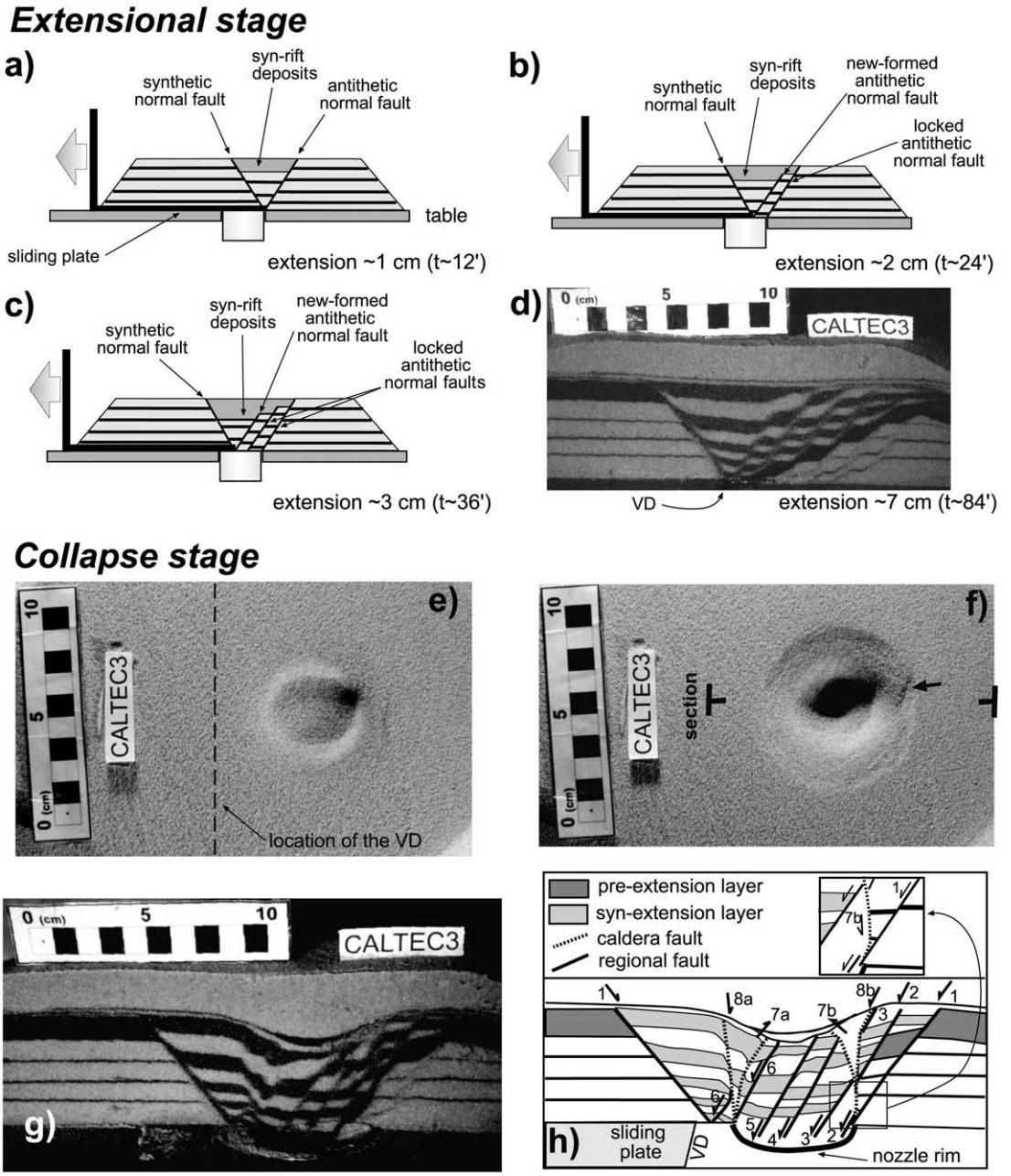

Fig. 3. Evolution of collapse experiment CALTEC 3. (a–d) Extension (section view) due to the outward migration of the VD generates an asymmetric graben, with 1 synthetic and several (the number depends upon the amount of extension) antithetic normal faults. The graben is filled with sand. (e–f) Collapse stages (map view): development of a first elliptic depression (e) and of a second concentric circular depression (f); the arrow in (f) shows the straight path of a portion of the outer depression. (g) Section view of the final stage of deformation. (h) Line drawing of section in (g); the numbers refer to the order of development of the faults, the arrows to their kinematics. Inset shows the reactivation of pre-existing normal faults by the reverse fault bordering the caldera.

out pre-existing structures on a very similar apparatus (Acocella et al., 2000) and the graben section in Fig. 3d. The comparison permitted to consider all the information necessary for the univocal interpretation of the cross sections of these experiments.

This procedure resulted in the line drawing in Fig. 3h. Here the caldera faults (dashed) are distinguished by the regional faults (solid lines). The graben, bordered by normal faults (numbers in Fig. 3h refer to their order of development) is dissected by the collapse structures. These are two concentric ring faults; the inner (faults 7) is a reverse ring fault, associated with the elliptic depression; the outer (faults 8) is a normal ring fault, associated with the circular depression. Previous caldera experiments showed that both the ring faults nucleated at the VD at the rim of the nozzle and then propagated upwards; in particular the reverse faults were outward dipping and the normal faults subvertical to inward dipping (Acocella et al., 2000). The pair of faults 7a and 8a (Fig. 3h) does not show any evident reactivation of the pre-formed regional normal faults. Conversely, the pair of ring faults 7b and 8b, as tangent in strike to fault 1, shows a partial reactivation (see inset in Fig. 3h) of the pre-existing normal fault 1. The reactivation is shown by the moderate outward propagation (inward dip) of the reverse fault 7b (Fig. 3h), which follows (for ~0.5 cm), in its bottom part, the path of the regional fault 1. Inward dipping normal fault 8b

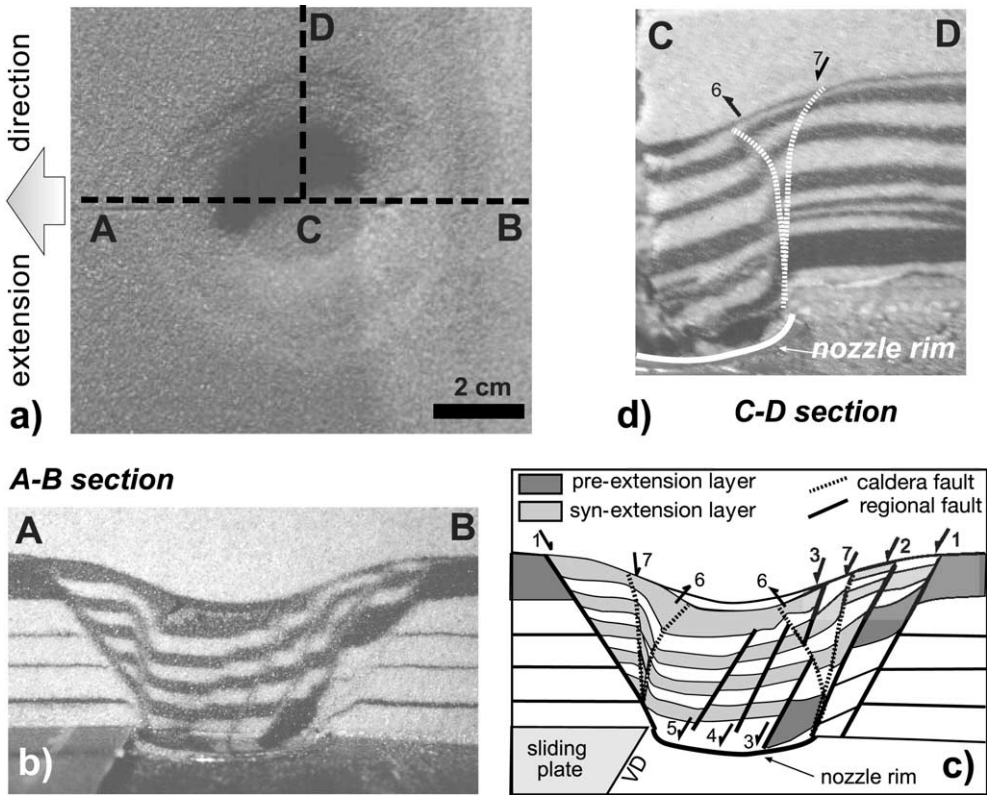

Fig. 4. Collapse experiment CALTEC 5. (a) Map view of the final stage of deformation. (b) Section view parallel to the extension direction. (c) Line drawing of the section, showing the reactivation of two normal faults during the development of the reverse ring fault, which is partly inward dipping. Reactivation occurs where the reverse fault strikes tangent to the regional faults. (d) Section view perpendicular to the extension direction; reactivation does not occur where regional faults are transverse to the reverse ring fault, which is outward dipping.

also reactivates, during collapse, pre-existing normal fault 3 at surface (Fig. 3h); this reactivation explains the partial straight path of the right part of the outer depression (see arrow in Fig. 3f).

A better example of reactivation is shown in the section view of CALTEC 5 (Fig. 4), with $T=5$ cm, $t_{ext}=60'$, for a total extension of 5 cm, the initial position of the VD at the left rim of the 5-cm-wide nozzle and $t_{col}=157'$. The evolution of this experiment is similar to that of CALTEC 3. The final stage of deformation shows two concentric depressions (Fig. 4a); the innermost has $E=0.80\pm0.04$ (Fig. 4a), the outermost is circular. Fig. 4b shows the section along the diameter of the caldera, parallel to the extension direction; the corresponding line drawing is shown in Fig. 4c: the reverse 6 and normal 7 ring faults dissect the graben (normal faults 1 to 5). The VD was here stopped, after 5 cm of extension, at the left rim of the nozzle; as a result, the synthetic normal fault is located at the rim of the nozzle.

The reverse ring fault 6 reactivates for $\sim$1 cm the regional faults 1 and 2 (Fig. 4c). This is shown by the outward propagation (inward dip) of the bottom of the reverse faults, following the paths of the tangent (along strike) and pre-existing inward-dipping normal faults (Fig. 4c). No reactivation is observed along a section perpendicular to the extension direction (section CD in Fig. 4d); the reverse fault, perpendicular to the pre-existing regional normal faults, is here constantly outward dipping.

Even though we tested different parameters, the collapse experiments are consistent with a similar evolution, which is characterised by an inner elliptic depression and an outer circular depression. The major axis of the elliptic depression is always parallel to the extension direction. The ellipticity of the depressions varies as a function of the number of reactivated faults (see Table 2); E is smaller ($\sim$0.8, as in CALTEC 5) when the reverse ring fault reactivates two tangent regional faults at opposite sides of the nozzle rim; E is larger ($\sim$0.9, as in CALTEC 3) when the ring fault reactivates 1 regional fault. The reactivation of the regional faults occurs only if these are very close (<3 mm) to the rim of the nozzle, that is where the reverse faults propagate.

3.2. Set 2: extension and resurgence

The second set simulates resurgence through the rise of the silicone. Here we present the results of 3 significant experiments (CALTEC 9, CALTEC 13, CALTEC 10), having different T/D ratios (between the thickness of the sand and the diameter of the nozzle). The T/D ratio is in fact considered a crucial parameter in controlling resurgence modalities (Acocella et al., 2001a).

Experiment CALTEC 9 has $T/D=1$, $t_{ext}=54'$, total extension of 4.5 cm, the initial position of the VD at 0.5 cm to the left of the right rim of the nozzle and the total duration of resurgence $t_{res}=191'$ (Fig. 5). The model extended for 4.5 cm, until the VD reached the opposite rim of the nozzle; this resulted in the formation of an asymmetric graben, bordered by 1 synthetic and 5 antithetic normal faults (Fig. 5a). After filling the graben with sand, the model underwent resurgence. A broad uplift formed at $t_{res}=60'$ (Fig. 5b). This is better developed at $t_{res}=120'$ (Fig. 5c), where the uplifted area attains an elliptic shape, with $E=0.89\pm0.03$. The major axis of the ellipse is perpendicular to the extension direction (parallel to the regional faults), which is converse to what was observed in collapse experiments. Two regional faults (4 and 5 in Fig. 5a) on the right part of the resurgent block are reactivated during the uplift (arrows in Fig. 5c). In the final stage ($t_{res}=180'$) of resurgence, the block is uplifted in portions bordered by three regional faults (see arrows in Fig. 5d).

The section view of the model through the diameter of the block and parallel to the extension direction is shown in Fig. 5e. The corresponding line drawing, obtained matching the section views of experimental resurgence without extension (Acocella et al., 2001a) and Fig. 5a, is shown in Fig. 5f. Here the regional faults (solid lines) and resurgence faults (dashed lines) are displayed; the numbers refer to their order of formation. Resurgence formed a reverse fault (dashed line 6a) and reactivated the pre-existing regional faults. Faults 4 and 5 were reactivated as normal faults; faults 3, 2 and (partly) 1 were reactivated as reverse faults (Fig. 5f). In particular, reverse fault 6b, which originated at the nozzle rim, propagated

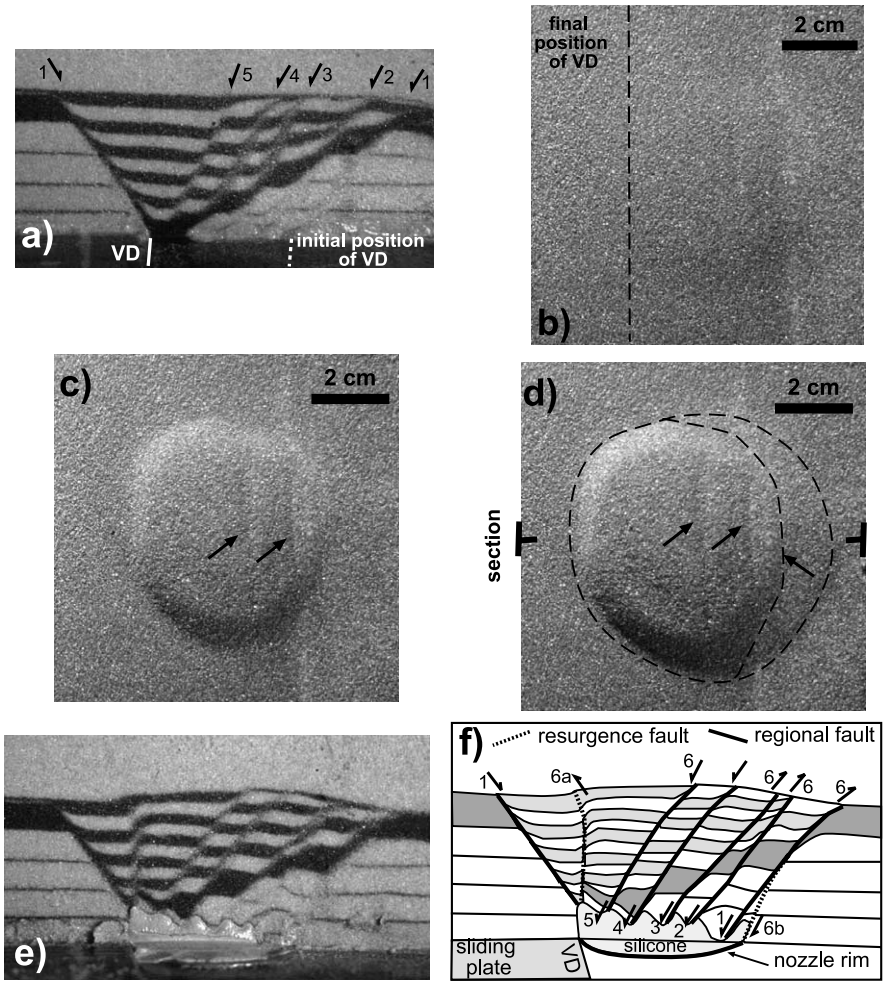

Fig. 5. Evolution of resurgence experiment CALTEC 9. (a) Section view after extension. (b) Map view of the early stage of resurgence. (c) The block becomes elliptical with the axis, perpendicular to the extension direction; arrows point to reactivated regional faults. (d) The final stage of deformation of the block shows an inner elliptic part and a subcircular outer uplifted area. (e) Section view of the experiment after resurgence. (f) Line drawing of the section; the numbers refer to the order of development of the faults, the arrows to their kinematics. The reverse fault bordering the block to the left is subvertical (dip ~88°).

upwards and met the upper portion of fault 1, then reactivated as a reverse fault.

There is a marked difference in the dip of the reverse faults in Fig. 5f: fault 6a is subvertical, possibly slightly outward dipping (dip ~88°), whereas fault 6b is inward dipping, (dip ~65°). During resurgence, reverse faults without previous extensional structures have a mean dip of 74°; subvertical reverse faults have never been observed (Acocella et al., 2001a).

A more evident case of difference in dip (and plunge) of the two reverse faults is shown in CALTEC 13 (Fig. 6), with $T/D = 1$, $t_{ext} = 15'$, for a total extension of 1.3 cm, the initial position of the VD at 4 cm to the left of the right rim of the nozzle and $t_{res} = 240'$ (Fig. 6). Extension here induced two opposite verging normal faults (1 in Fig. 6a). The synthetic normal fault 1 is located at 0.5 cm outside the nozzle rim; the antithetic normal fault 1 is located in line with the nozzle rim.

The evolution of the resurgence is similar to

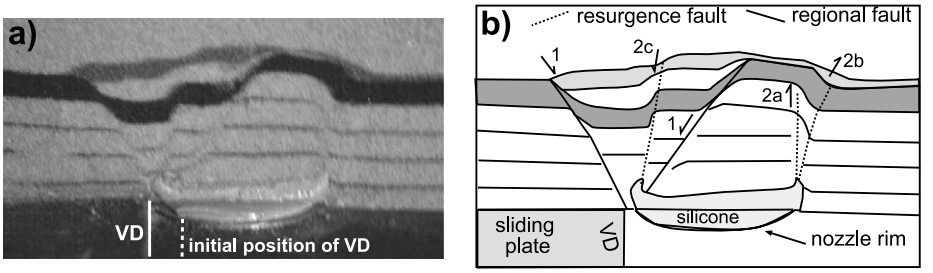

Fig. 6. Section view (a) and related line drawing (b) of experiment CALTEC13 after extension and resurgence. The fault bordering the block to the left (2c) is normal and outward dipping (dip ~75°).

CALTEC 9, with an elliptic block ($E = 0.83 \pm 0.05$). The section of CALTEC 13 (Fig. 6b) shows two regional faults (1) and three resurgence faults. Normal fault 2a is partly developed and is related to late resurgence, where gravity sliding occurs (Acocella et al., 2001a). The dip and plunge of the inward dipping fault 2b is consistent with differential uplift (Acocella et al., 2001a); however, fault 2c, supposed to be an inward dipping reverse fault, is an outward dipping normal fault (dip ~75°).

We now consider experiment CALTEC 10 with $T/D = 0.6$, $t_{ext} = 64'$, for a total extension of 5 cm, the initial position of the VD at the right rim of the nozzle and $t_{res} = 183'$ (Fig. 7). The section view of the graben at the end of extension is shown in Fig. 7a. The VD (and fault 1) is located in correspondence with the nozzle rim; the normal fault 6 is located at 0.7 cm from the rim. After resurgence, the final stage of deformation is shown in Fig. 7b. A dome is formed; two regional faults (indicated by arrows) were reactivated, bordering an elongated crestal depression, parallel to the VD. The resurgent dome is subcircular in map view.

Section view in Fig. 7c shows a similar deformation pattern as in CALTEC 9 (Fig. 5). Reverse fault 7 has a different plunge from fault 2c in Fig. 6b (slightly inward dipping, dip ~80°). Regional faults 6 and 5 were reactivated during resurgence as reverse and normal faults, respectively, bordering the crestal depression (Fig. 7c).

Not considering smaller scale perturbations due to the activity of the faults, the overall shape of the rising silicone is domed, with the topmost part

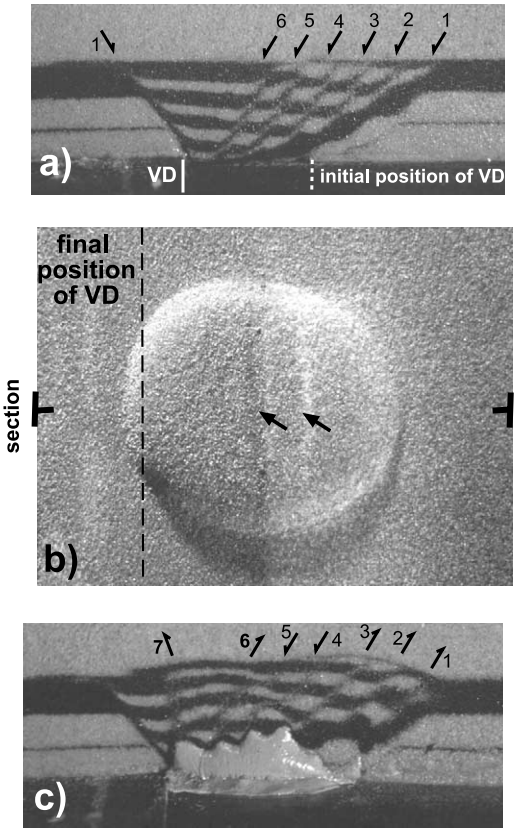

Fig. 7. Evolution of resurgence experiment CALTEC 10. (a) Section view of the experiment after extension. (b) Map view of the final stage of resurgence; arrows show the elongated crestal depression bordered by regional faults. (c) Section view of the experiment after resurgence; the overburden shows a domed structure, as the overall topmost part of the rising silicone. The fault bordering the block to the left (7) is reverse and inward dipping (dip ~80°).

in the centre. The layers in the overburden are also domed. This is different from what was observed in experiments CALTEC 9 and CALTEC 13 ($T/D = 1$), where the overall shape of silicone was rising at the sides of the block or flat, respectively.

3.3. Set 3: extension, collapse and resurgence

The third set (2 experiments) simulates resurgence over collapse, with different amounts of pre-collapse extension (1 and 5 cm). The two experiments are consistent and the results of CALTEC 11 are briefly presented. CALTEC 11 has $T/D = 1$, the total duration of extension $t_{ext} = 64'$, for a total extension of 5 cm, the initial position of the VD at the right rim of the nozzle, the total duration of collapse $t_{col} = 180'$ and the total duration of resurgence $t_{res} = 240'$. Section view after extension shows 1 synthetic and 5 antithetic normal faults (Fig. 8a). The map view after collapse shows two concentric depressions (Fig. 8b); the innermost has $E = 0.81 \pm 0.08$; the outermost is subcircular, even though partially confined by two regional faults on the right (arrows in Fig. 8b), similarly to Fig. 3f. The final stage of deformation, after resurgence, shows an elliptic block ($E = 0.87 \pm 0.05$) within the outer caldera. The major axis of the resurgent block (Fig. 8c) is orthogonal to the major axis of the ellipse forming the inner caldera (Fig. 8b).

Section view shows that the caldera and resurgence structures are confined in two shear zones (fault zones 6 in Fig. 8d). The comparison with experiments previously performed without pre-existing structures (Acocella et al., 2000) suggests that the zone to the left is made up of: the subvertical ring fault of the outer caldera, not reactivated during resurgence (Fig. 8c); the outward dipping fault, formed as a reverse fault during collapse and reactivated as normal during resurgence. The zone to the right is made up of: (1) the inward dipping ring fault of the outer caldera, which reactivated the regional normal fault at its top (Fig. 8b), and has been then reactivated as reverse fault during resurgence (Fig. 8c); (2) the subvertical reverse fault formed during collapse and reactivated as normal during resurgence.

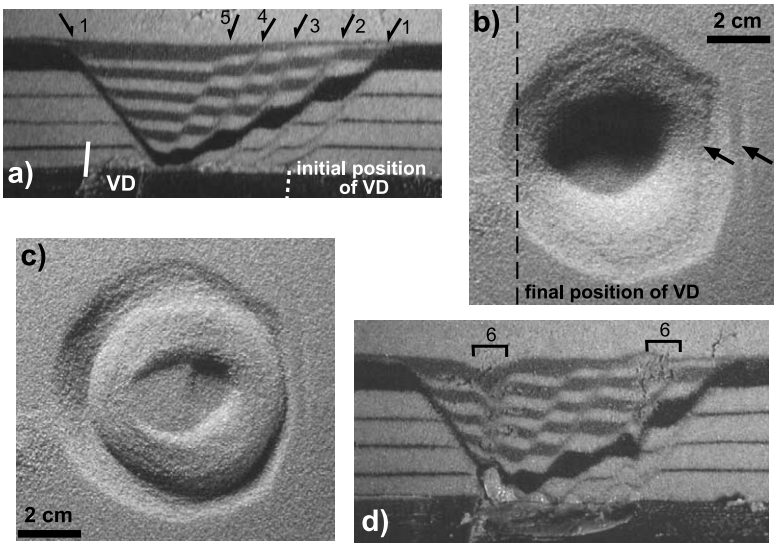

Fig. 8. Evolution of extension+collapse+resurgence (CALTEC 11). (a) Section view of the experiment after extension. (b) Map view of the final stage of collapse; arrows show the confinement of the outer caldera due to regional faults. (c) Map view of the final stage, after resurgence; resurgence partly reactivates the inner caldera boundary (to the left), partly the outer boundary (to the right). (d) Section view of the experiment; both the caldera and the resurgence faults occur in the same narrow shear zones (6).

4. Discussion

4.1. Interpretation of the experiments

Collapse over extension showed that, similarly to collapses without pre-existing extensional structures, a reverse and a normal ring fault formed; their overall evolution and mechanical interpretation were previously discussed (i.e. Acocella et al., 2000). Here we focus on two main novelties related to the regional extension: (1) the inner caldera is elliptic, with the major axis parallel to the extension direction (Figs. 3 and 4); (2) during collapse, the reverse faults bordering the depression reactivate, becoming slightly inward dipping, the regional normal faults, if these are close (<0.3 cm). Depending on such a distance, one or two regional faults along the nozzle rim (Figs. 3h and 4c, respectively) may be reactivated. Experiments without reactivation have not been observed. The reactivated regional faults are tangent in strike to the reverse ring faults and no reactivation is observed on sections perpendicular to the extension direction (Fig. 4d). The smaller eccentricities ($E\sim0.8$) are related to the calderas where both reverse faults reactivate the regional normal faults (Table 2). Conversely, higher eccentricities ($E\sim0.9$) are related to the reactivation of only 1 regional fault. Every reactivated regional fault induces a decrease in the eccentricity of ~0.1.

We propose that the eccentricity of the inner ring fault, which is the structural boundary of the collapses, is related to the partial reactivation (with a limited outward propagation of the reverse faults) of the regional faults during collapse (Fig. 9). As a result, along this direction, the caldera gets wider than expected (Fig. 9b). No reactivation occurs where the reverse faults are transverse to the regional faults. Here the reverse faults are outward dipping and the caldera is narrower (Fig. 9c). This results in an elliptic caldera at surface, parallel to the extension direction. The outer caldera is usually circular, even though it may be partly shaped on pre-existing normal faults (Figs. 3f and 8b).

Resurgence over pre-existing extensional structures showed overall similarities with models without the extensional structures. In fact, the same architecture is observed as a function of the aspect ratio (height T/width D) of the overburden. For $T/D\sim1$ a resurgent block forms; for $T/D\sim0.6$ a resurgent dome forms, similarly to what was observed in Acocella et al. (2001a). We refer to this work for the interpretation of these deformation patterns. The overall shape of uprising silicone is also partly dependent on the T/D ratio. For lower ratios, the silicone forms a dome and its maximum uplift is located in the centre (Fig. 7), whereas for higher ratios the silicone rises more at the sides (Figs. 5 and 6). These similarities show that pre-existing discontinuities do not affect the overall architecture of resurgent domes.

The main novelties of the resurgence models are: (1) the uplifted parts are elliptic, with the major axis orthogonal to the extension direction (Figs. 5 and 6); (2) the crestal depression (for experiments with $T/D<0.6$, as in Fig. 7b) is elongated (rather than circular) and bordered by regional faults; (3) the faults bordering the uplifted part, which should be inward dipping (Acocella et al., 2001a), with a reverse displacement, are here subvertical (Figs. 5 and 6) or even outward dipping, with a normal displacement (Fig. 6).

The change in the plunge of the reverse faults (which thus become normal) occurs when these are near (<0.3 cm) to an outward dipping regional fault. This is, in fact, able to perturb the stress field of the newly formed reverse fault, inducing a change of plunge from inwards to outwards, forming a normal fault (Fig. 6). On the right side of the uplifted block, resurgence occurs forming a reverse fault (if no regional fault is present; Fig. 6) or (totally or in part) reactivating a regional fault (if regional faults were already formed; Fig. 5). Such a reactivation occurs if the regional fault is suitably oriented (same plunge and similar dip) and tangent to the reverse fault. Reactivation of the regional faults as normal faults during resurgence has also been observed on the faults within the uplifted part (Fig. 5).

Thus, pre-existing regional structures can control the development of the reverse faults bordering the uplifted part in two ways: (1) if they are

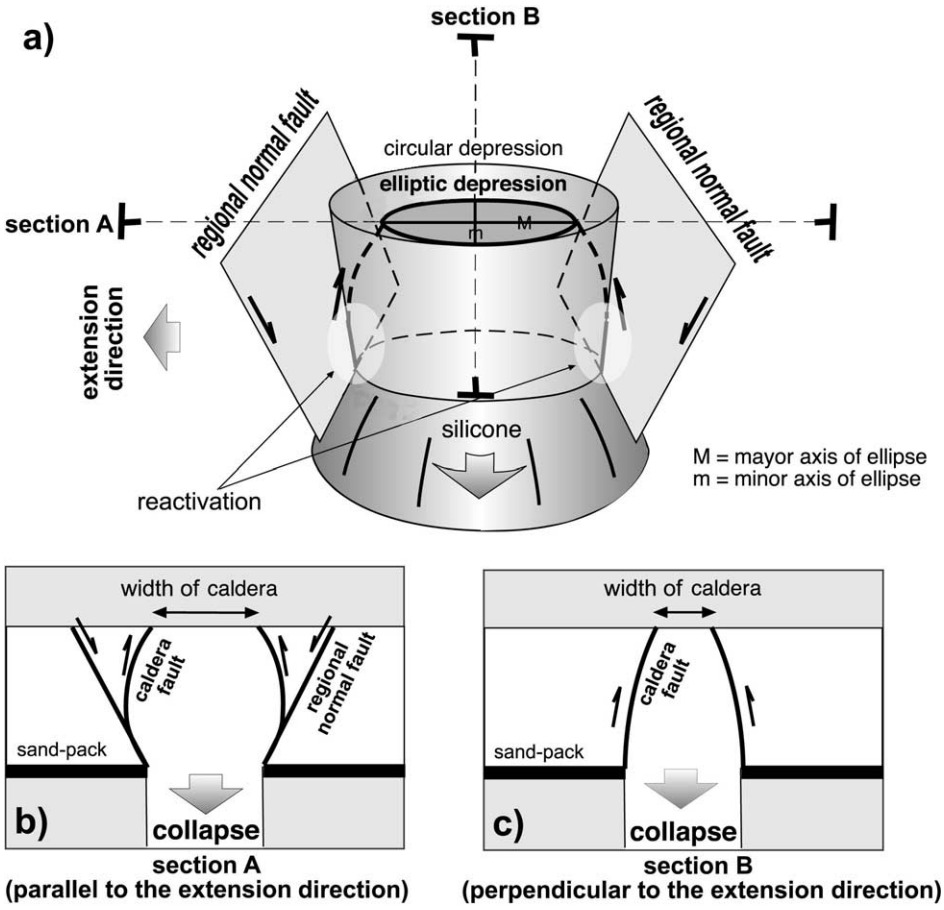

Fig. 9. (a) Proposed mechanism for the reactivation of regional faults during collapse and for the elongation of the caldera parallel to the extension direction. (b) The reverse faults, where tangent in strike to the regional faults, become partly inward dipping, inducing a wider depression on the corresponding parts at surface. (c) No reactivation is observed when the regional faults are transverse to the reverse faults.

opposite verging, by inducing a change in the plunge of the expected reverse faults, forming normal faults (fault 2c in Fig. 6); (2) if their plunge is consistent, by the partial or total reactivation of the regional faults during the development of the reverse faults (fault 6 in Fig. 5f). Table 2 shows that the more pronounced elliptic resurgences (smaller eccentricities) are due to the change in plunge of the reverse fault, which becomes a normal fault. The different plunge of the fault shifts the structural boundary of the uplifted part in an inner position, resulting in an elliptic resurgence (Fig. 10). We interpret the ellipticity of the resurgences as due to the change in the plunge of the reverse fault into a normal fault on one side of the block. The reactivation of the regional fault as a reverse fault (as fault 6b in Fig. 5f) during resurgence does not significantly affect the ellipticity of the uplifted part.

The experiments regarding resurgence over collapse under previous extension show the reactivation of the former caldera faults during resurgence. Even though the modalities of development of the caldera faults are partly controlled by the pre-existing regional structures, the modalities of reactivation of the caldera faults during resurgence are identical to the ones observed without a regional extension (Acocella et al., 2000).

Both experimental collapse and resurgence under previous extension thus showed similar fea-

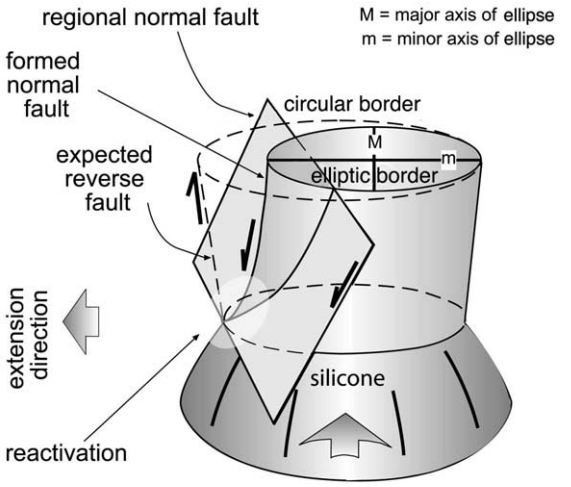

Fig. 10. Proposed mechanism for the reactivation of regional faults during resurgence and for the elongation of the uplifted part perpendicular to the extension direction. The reverse fault to the left, where tangent in strike to the regional faults, becomes partly outward dipping (rather than inward dipping, as expected), inducing a narrower uplifted area on the corresponding part at surface.

tures. Even though with different modalities, the reverse faults partly reactivated the regional faults during differential uplift; this resulted in elliptic calderas and resurgences at surface. The normal faults, which accommodated the deformation induced by the reverse faults, did not significantly affect the shape of the collapses, domes and blocks at surface. This confirms that the reverse faults developed during differential uplift are the structural border of the depressions and uplifted part (Acocella et al., 2000).

4.2. Modalities of reactivation

The modalities of reactivation of pre-existing normal faults during collapse and resurgence are schematically shown, for consistent and opposite plunges with regard to the regional faults, in Fig. 11a. The solid line reports the dip in section view of a regional fault, the dashed line the dip of the expected normal and reverse faults in collapses and resurgences without extension (Acocella et al., 2000) and the dotted line shows the dip of the observed normal and reverse faults after extension. The mean dip of the regional normal faults in the experiments is $57° \pm 5°$. The mean dips of the reverse faults and normal faults during collapse and resurgence (without extension) are $74° \pm 10°$ and $78° \pm 7°$, respectively. Regional faults thus have lower dips than the expected reverse and normal faults.

Two different modalities of reactivation have been observed. (1) A partial reactivation (branching) of the pre-existing regional faults during the development of both normal and reverse faults in the experiments. This is characterised by the branching of the normal or reverse faults during collapse or resurgence at the base of a previous normal fault (A, D and H in Fig. 11a); thus, the regional fault was able to partially control the dip or the plunge of the normal and reverse faults during collapse and of the reverse faults during resurgence. This is the proposed mechanism responsible for elliptic calderas and resurgences. (2) The total reactivation of regional structures during the development of normal and reverse faults, with the same plunge, during resurgence (E and G in Fig. 11a).

The branching of the normal and reverse faults on the regional structures has been observed both during collapse and resurgence. Conversely, the complete reactivation of normal and reverse faults has been observed only during resurgence, when two conditions occur: (1) the resurgence faults have the same plunge as the regional faults, and (2) the reactivation of a regional fault as reverse is connected with the reactivation of another regional fault as normal or vice-versa (Figs. 5 and 7). Thus, in the second condition, complete reactivations in resurgence occur only in pairs, with 1 normal and 1 reverse fault. If both conditions occur, the reactivation occurs also with differences up to 20° between the dip of the regional and resurgence faults.

This interdependent, total reactivation of regional faults with the same plunge gives an overall asymmetry to the uplifted part. The fact that this feature is not observed in collapses suggests that, during uplift, space can be more easily accommodated (allowing a total reactivation of the faults), with a higher degree of freedom (development of asymmetric blocks). We interpret this different resolution of the space problem during resurgence

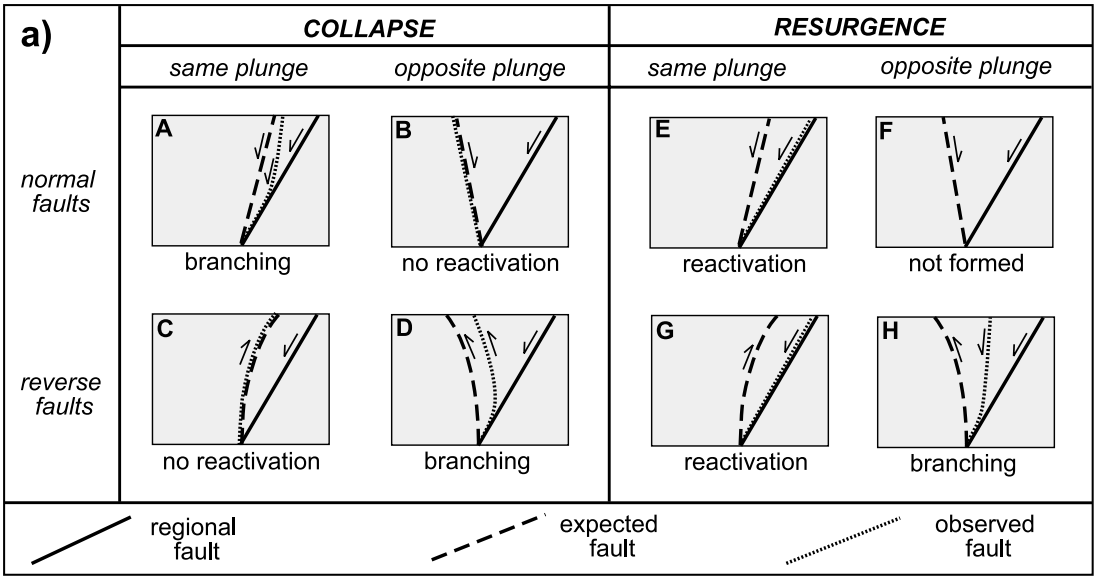

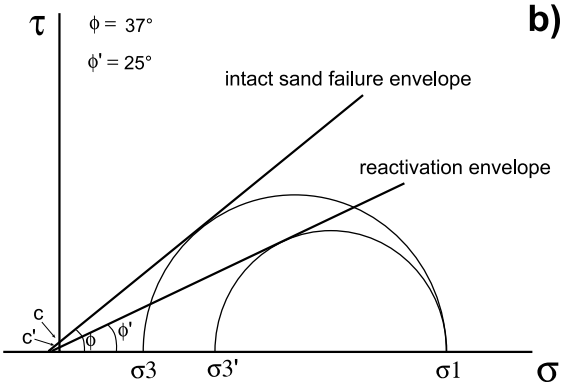

Fig. 11. (a) Modalities of reactivation of the pre-existing normal faults during the development of the normal and reverse faults in collapse and resurgence. Branching is characterised by a common path of the bottom of the regional faults and the caldera and resurgence faults. Conversely, a complete reactivation of the regional faults occurs only during resurgence. (b) Schematic Mohr–Coulomb diagram showing the relationships between the intact failure envelope of the used sand and the (complete) reactivation envelope: values of the cohesion (c'), angle of internal friction (ϕ') and $\sigma 3'$ vary accordingly.

and collapse as responsible for the observed difference in the occurrence of branching or total reactivation modalities.

The observed, total reactivation of the regional faults during differential uplift is the result of the local decrease in the shear strength $\tau = \sigma\mu + c$, where σ is the normal effective stress, μ is the static coefficient of rock friction ($\mu = \tan\phi$, where ϕ is the angle of internal friction) and c is the cohesion. The decrease in shear strength may be related to the loss in cohesion c and a drop in the friction coefficient μ. The loss of cohesion, given the low cohesion (few hundreds of Pa) of the dry sand we used is assumed to be negligible. The drop in the friction coefficient μ is related to the decrease of the angle of internal friction ϕ within the dilatancy zone created by the fault. The drop in μ has been previously observed experimentally and has been estimated as $\sim$30% (Faccenna et al., 1995). Fig. 11b shows the qualitative relation-

ships between the intact ($\phi = 37°$) and the reactivated ($\phi' = 25°$) envelope in a Mohr–Coulomb diagram. The difference in shear strength is mostly attributed to the loss ($\sim 30\%$) in the friction coefficient and, to a much lesser extent, to the drop in cohesion. In our experiments, the reactivated normal faults had a dip of $57° \pm 5°$; theoretical calculations predict that pre-existing normal faults dipping less than 50° become highly inhibited for reactivation (Sibson, 1985).

4.3. Comparison with nature

A detailed and specific comparison with nature is beyond the purpose of this paper. Here we briefly address some points of interest for a general application of our experiments.

As far as calderas are concerned, their ellipticity has been related to the collapse of an elongated underlying magma chamber or post-caldera extension. In the first case, the minimum regional stress field orientation is responsible for a borehole breakout mechanism for the elongation of magma chambers parallel to the extension direction (Kenya Rift; Bosworth et al., 2000); alternatively, pre-existing transverse structures, reactivated during extension, enhance the elongation of magma chambers and thus calderas at surface (Ethiopian Rift; Acocella et al., 2002). In the second case, the ellipticity of calderas has been explained as a consequence of the activity of post-caldera rift faults and the magma chamber does not necessarily have to be elliptic (Fieale volcano, Afar; De Chabalier and Avouac, 1994).

Our experiments suggest a further explanation for the ellipticity of calderas and show that, because of the reactivation of pre-existing structures, elliptic calderas may develop from circular magma chambers. These results can be applied to elliptic calderas with moderate (up to few hundreds of metres) subsidence or, in the case of larger (up to thousands of metres) subsidence, only to the inner ring fault system. In fact, in the first case, only an elliptic ring fault forms (i.e. Fig. 3e). In the second case, two ring systems form, but only the inner is elliptic (i.e. Fig. 3f).

Even though the assessment of the shape of a magma chamber is essential for an accurate application of our experiments, calderas elongated parallel to the extension direction in narrow rift zones without pre-existing transverse structures (such as on newly-formed oceanic crust) may be the best candidates for comparison. For example, the oceanic ridge of Iceland is formed on a non-fractured crust and is characterised by calderas with a moderate subsidence; among these, Torfajokull, Kverkfjoll, Oskjuvatn (Askja) and Krafla calderas are elliptic and elongated parallel to the extension direction (Newhall and Dzurisin, 1988, and references therein; Gudmundsson and Backstrom, 1991). In this framework, our experiments may be of interest to understand further the structure of these Icelandic calderas and the role of regional extension on their development.

As far as resurgence is concerned, analogously to what pointed out with calderas, the experiments permit to understand the structure of elongated resurgences with previous extensional structures. Since resurgence is absent in calderas along oceanic rift zones, comparison has to be made with continental rifts, taking into account the possible role of pre-existing transverse structures. Nevertheless, all the major resurgences in continental extensional zones show a confinement or elongation of the uplifted area due to regional structures, such as at Ischia (Acocella and Funiciello, 1999), Campi Flegrei (Orsi et al., 1996), La Pacana (Lindsay et al., 2001) and Cerro Galan (Riller et al., 2001) or the elongation of the crestal depression, in line with regional systems, such as Valles (Nielson and Hulen, 1984; Self et al., 1986) and Long Valley (Bailey et al., 1976; Goldstein and Stein, 1988).

Moreover, resurgence experiments show that, under regional extension, no continuous reverse ring fault is required, as this may partly be a normal fault. This means that the space required to accommodate the uplift during resurgence may be created by the activity of a single ring structure, partly reverse and partly normal. This mechanism finds close similarities with previous proposed resurgence mechanisms. In fact, a simple shear mechanism for resurgence was proposed for the resurgent blocks of Ischia, Pantelleria (Orsi et al., 1991) and Campi Flegrei (Orsi et al., 1996). According to this model, extension on

one side of the block accommodated compression on the opposite side. Even though our experiments are related to a pure-shear mechanism and do not simulate simple shear (without significant internal block rotations), the overall geometry and kinematics of this model is consistent with our results. Similar models, with subvertical normal faults on one side of the block and normal faults on the opposite, have also been proposed for resurgence at Ischia (Tibaldi and Vezzoli, 1998; Tibaldi and Vezzoli, 2000).

5. Conclusions

The collapse experiments under previous extension showed inner elliptic depressions with the major axis parallel to the extension direction. The partial reactivation of the pre-existing normal faults was observed during the development of the caldera reverse faults, which partly became inward dipping. Resurgence under previous extension also showed a moderate elongation of the uplifted part, with the main axis perpendicular to the extension direction. At depth, pre-existing normal faults were partly reactivated by the reverse faults formed during resurgence; these became locally outward dipping, with a normal throw. The experiments suggest that the observed elongation of calderas and resurgences is the result of the reactivation of pre-existing structures during a differential uplift. This reactivation resulted in elliptic calderas (major axis parallel to the extension direction) and resurgences (major axis perpendicular to the extension direction) at surface. The results suggest that elliptic calderas and resurgences may develop even with circular magma chambers.

Acknowledgements

The authors wish to thank F. Cifelli for invaluable assistance during the run of the experiments and C. Faccenna for useful suggestions on reactivation. The reviewers H. Komuro, O. Roche and the editor T. Koyaguchi provided useful comments and suggestions. The work was carried out within the GNV framework program (project no. 16).

References

Acocella, V., Funiciello, R., 1999. The interaction between regional and local tectonics during resurgent doming: The case of the island of Ischia, Italy. J. Volcanol. Geotherm. Res. 88, 109–123.

Acocella, V., Cifelli, F., Funiciello, R., 2000. Analogue models of collapse calderas and resurgent domes. J. Volcanol. Geotherm. Res. 104, 81–96.

Acocella, V., Cifelli, F., Funiciello, R., 2001a. The control of overburden thickness on resurgent domes: Insights from analogue models. J. Volcanol. Geotherm. Res. 111, 137–153.

Acocella, V., Cifelli, F., Funiciello, R., 2001b. Formation and architecture of nested collapse calderas: Insights from analogue models. Terra Nova 13, 58–63.

Acocella, V., Korme, T., Salvini, F., Funiciello, R., 2002. The control of transverse tectonics on caldera development in the Ethiopian Rift. J. Volcanol. Geotherm. Res. 119, 189–203.

Bailey, R.A., Dalrymple, G.B., Lanphere, M.A., 1976. Volcanism, structure, and geochronology of Long Valley Caldera, Mono County, California. J. Geophys. Res. 81, 725–744.

Bosworth, W., Burke, K., Strecker, M., 2000. Magma chamber elongation as an indicator of intraplate stress field orientation: 'Borehole breakout mechanism' and examples from the Late Pleistocene to Recent Kenya Rift Valley. In: Jessel, M.W., Urai, J.L. (Eds.), Stress, Strain and Structure, A Volume in Honour of W.D. Means. J. Virtual Explor. 2.

Civetta, L., Cornette, Y., Gillot, P.Y., Orsi, G., 1988. The eruptive history of Pantelleria (Sicily Channel) in the last 50 ka. Bull. Volcanol. 50, 47–57.

De Chabalier, J.B., Avouac, J.P., 1994. Kinematics of the Asal Rift (Djibouti) determined from the deformation of Fieale Volcano. Science 265, 1677–1681.

Donnadieu, F., Merle, O., 1998. Experiments on the indentation process during cryptodome intrusions: New insights into Mount St. Helens deformation. Geology 26, 79–82.

Druitt, T.H., Sparks, R.S., 1984. On the formation of calderas during ignimbrite eruptions. Nature 310, 679–681.

Faccenna, C., Nalpas, T., Brun, J.P., Davy, P., Bosi, V., 1995. The influence of pre-existing thrust faults on normal fault geometry in nature and in experiments. J. Struct. Geol. 17, 1139–1149.

Goldstein, N.E., Stein, R.S., 1988. What's new at Long Valley. J. Geophys. Res. 93, 13187–13190.

Gudmundsson, A., 1988. Formation of collapse calderas. Geology 16, 808–810.

Gudmundsson, A., 1998. Formation and development of normal-fault calderas and the initiation of large explosive eruptions. Bull. Volcanol. 60, 160–170.

Gudmundsson, A., Marti, J., Turon, E., 1997. Stress fields generating ring faults in volcanoes. Geophys. Res. Lett. 24, 1559–1562.

Gudmundsson, A., Backstrom, K., 1991. Structure and development of the Sveinagja graben, northeast Iceland. Tectonophysics 200, 111–125.

Hailermariam, H., Mulugeta, G., 1998. Temperature-dependent rheology of bouncing putties used as rock analogs. Tectonophysics 294, 131–141.

Henry, C.H., Price, J.G., 1984. Variations in caldera development in the tertiary volcanic field of Trans-Pecos Texas. J. Geophys. Res. 89, 8765–8786.

Hubbert, M.K., 1937. Theory of scale models as applied to the study of geologic structures. Bull. Geol. Soc. Am. 48, 1459–1520.

Kennedy, B., Stix, J., Lavallée, Y., Vallance, J., 1999. Controls on caldera structure and morphology: Results from experimental simulations. EOS Trans. Am. Geophys. Union 80, F1121.

Komuro, H., 1987. Experiments on cauldron formation: A polygonal cauldron and ring fractures. J. Volcanol. Geotherm. Res. 31, 139–149.

Krantz, R.W., 1991. Measurements of friction coefficients and cohesion for faulting and fault reactivation in laboratory models using sand and sand mixtures. In: Cobbold, P.R. (Ed.), Experimental and Numerical Modelling of Continental Deformation. Tectonophysics 188, pp. 203–207.

Lindsay, J.M., de Silva, S., Trumbull, R., Emmermann, R., Wemmer, K., 2001. La Pacana caldera, N. Chile a re-evaluation of the stratigraphy and volcanology of one of the world's largest resurgent calderas. J. Volcanol. Geotherm. Res. 106, 145–173.

Lipman, P.W., 1984. The roots of ash flow calderas in Western North America: Windows into the tops of granitic batholiths. J. Geophys. Res. 89, 8801–8841.

Lipman, P.W., 1997. Subsidence of ash-flow calderas: Relation to caldera size and magma-chamber geometry. Bull. Volcanol. 59, 198–218.

Marsh, B.D., 1984. On the mechanics of caldera resurgence. J. Geophys. Res. 89, 8245–8251.

Marti, J., Ablay, G.J., Redshaw, L.T., Sparks, R.S.J., 1994. Experimental studies of collapse calderas. J. Geol. Soc. Lond. 151, 919–929.

Merle, O., 1998. Internal strain within lava flows from analogue modelling. J. Volcanol. Geotherm. Res. 81, 189–206.

Merle, O., Vendeville, B., 1995. Experimental modelling of thin-skinned shortening around magmatic intrusions. Bull. Volcanol. 57, 33–43.

Newhall, C.G., Dzurisin, D., 1988. Historical Unrest at Large Calderas of the World. U.S. Geological Survey, 1109 pp.

Nielson, D.L., Hulen, J.B., 1984. Internal geology and evolution of the Redondo Dome, Valles Caldera, New Mexico. J. Geophys. Res. 89, 9695–9711.

Opheim, J.A., Gudmundsson, A., 1989. Formation and geometry of fractures and related volcanism of the Krafla fissure swarm, Northeast Iceland. Geol. Soc. Am. Bull. 101, 1608–1622.

Orsi, G., De Vita, S., di Vito, M., 1996. The restless, resurgent Campi Flegrei nested caldera (Italy): Constrains on its evolution and configuration. J. Volcanol. Geotherm. Res. 74, 179–214.

Orsi, G., Gallo, G., Zanchi, A., 1991. Simple-shearing block resurgence in caldera depressions. A model from Pantelleria and Ischia. J. Volcanol. Geotherm. Res. 47, 1–11.

Ramberg, H., 1981. Gravity, Deformation and the Earth's Crust, 2nd ed. Academic Press, London, 452 pp.

Riller, U., Petrinovic, I., Ramelow, J., Strecker, M., Oncken, O., 2001. Late Cenozoic tectonism, collapse caldera and plateau formation in the central Andes. Earth Planet. Sci. Lett. 188, 299–311.

Roche, O., Druitt, T.H., Merle, O., 2000. Experimental study of caldera formation. J. Geophys. Res. 105, 395–416.

Scandone, R., 1990. Chaotic collapse of calderas. J. Volcanol. Geotherm. Res. 42, 285–302.

Schellart, W.P., 2000. Shear test results for cohesion and friction coefficients for different granular materials: Scaling implications for their usage in analogue modelling. Tectonophysics 324, 1–16.

Self, S., Goff, F., Gardner, J.N., Wright, J.V., Kite, W.M., 1986. Explosive rhyolitic volcanism in the Jemez Mountains: Vent locations, caldera development and relation to regional structure. J. Geophys. Res. 91, 1779–1798.

Sibson, R.H., 1985. A note on fault reactivation. J. Struct. Geol. 7, 751–754.

Smith, R.L., 1979. Ash-flow magmatism. Geol. Soc. Am. Spec. Pap. 180, 5–27.

Smith, R.L., Bailey, R.A., 1968. Resurgent cauldrons. Geol. Soc. Am. Mem. 116, 613–662.

Talbot, C.J., 1999. Can field data constrain rock viscosities? J. Struct. Geol. 21, 949–957.

Tibaldi, A., Vezzoli, L., 1998. The space problem of caldera resurgence: An example from Ischia Island, Italy. Geol. Rundsch. 87, 53–66.

Tibaldi, A., Vezzoli, L., 2000. Late Quaternary monoclinal folding induced by caldera resurgence at Ischia, Italy. In: Cosgrove, J.W., Ameen, M.S. (Eds.), Forced Folds and Fractures. Geol. Soc. Lond. Spec. Publ. 169, pp. 103–113.

Troll, V.R., Walter, T.R., Schmincke, H.U., 2002. Cyclic caldera collapse: Piston or piecemeal subsidence? Field and experimental evidence. Geology 30, 135–138.

Walker, G.P.L., 1988. Three hawaiian calderas: An origin through loading by shallow intrusions? J. Geophys. Res. 93, 14773–14784.

Walter, T.R., Troll, V.R., 2001. Formation of caldera periphery faults: An experimental study. Bull. Volcanol. 63, 191–203.

Weijermars, R., Jackson, M.P.A., Vendeville, B., 1993. Rheological and tectonic modeling of salt provinces. Tectonophysics 217, 143–174.

Williams, H., 1941. Calderas and their origin. Calif. Univ. Publ. Geol. Sci. Bull. 21, 239–346.

Withjack, M.O., Scheiner, C., 1982. Fault patterns associated with domes – An experimental and analytical study. AAPG Bull. 66, 302–316.